A&A 422, 717–729 (2004)
DOI: 10.1051/0004-6361:20040159

Astronomy & Astrophysics

Gas and dust in Comet C/2000 WM1 during its closest approach to Earth: Optical imaging and long-slit spectroscopy

L.-M. Lara[1], G. P. Tozzi[2], H. Boehnhardt[3], M. DiMartino[4], and R. Schulz[5]

[1] Instituto de Astrofísica de Andalucía, CSIC, PO Box 3004, 18080 Granada, Spain
e-mail: lara@iaa.es
[2] INAF, Osservatorio Astrofisico di Arcetri, Largo E. Fermi 5, 50125 Firenze, Italy
e-mail: tozzi@arcetri.astro.it
[3] Max-Planck-Institut für Astronomie, Königstuhl 17, 69117 Heidelberg, Germany
e-mail: hboehnha@mpia-hd.mpg.de
[4] INAF, Osservatorio Astronomico di Torino, 10025 Pino Torinese (TO), Italy
e-mail: dimartino@to.astro.it
[5] Research and Scientific Support Department of ESA, ESTEC, Keplerlaan 2, 2200AG Noordwijk, The Netherlands
e-mail: Rita.Schulz@esa.int

Received 2 June 2003 / Accepted 17 April 2004

Abstract. We have investigated the dust and gas coma of the comet C/2000 WM1 (LINEAR) during Dec. 2–4, 2001, its closest approach to Earth. The gaseous coma is slightly asymmetric in CN and C_2, indicating the presence of some structures which are detected either by applying enhancement techniques or studying the azimuthal distribution of material. This asymmetry is due to the existence of a double jet in a direction almost perpendicular to the Sun–comet direction. These structures are not clearly detected in C_3. The morphological analysis of the dust coma shows a faint, short and narrow sunward structure, besides the dust tail in a position angle of ∼60°.

CN is produced at a rate of 2.43×10^{26} s^{-1} with lifetimes that can be considered as representative of HCN being the parent species. In the case of C_2, the use of usual lifetimes (τ_p, τ_d) requires a modified two-steps photolytic model to account for the pronounced flatness of the column density profile in the inner coma. Usual steady-state model gives rise to a $Q_{C_2} = 3.11 \times 10^{26}$ s^{-1}. Other gas species as C_3 and NH_2 have been also detected from the spectrum, although with a lower S/N. The computed production rates are 3.6×10^{24} s^{-1} and 2.15×10^{26} s^{-1}, respectively. Determination of the CN and C_2 production rates by means of the Haser modeling (Haser 1957) with customary scalelengths indicates that C/2000 WM1 is a C_2-enriched comet at 1.178 AU heliocentric distance. The dust production rate, parameterised by $A(\theta)f\rho$, is ∼300–400 cm when measured in two continuum regions, centered at 4845 and 6840 Å, whilst this value is slightly lower in Bessel R and Gunn i (∼230 cm). Thus, the gas-to-dust mass ratio is in the order of 6.3, a relatively gassy comet.

The surface brightness profiles of the continuum, either azimuthally averaged profiles from the broadband images or in east–west direction from the long-slit spectrum, can be well fitted with $m \approx 1$ in $\log B - \log \rho$ representation. On the other hand, the study of the dust coma as imaged with the broadband and narrowband filters reveals that variations in the size and/or composition of the grains might be occurring while traveling outward. This fact is manifested as a sharp decrease of $\sum Af$ vs. ρ at $700 \leq \rho \leq 15\,000$ km. The fit of these $\sum Af$ profiles vs. ρ points to the existence of two different grain populations with their own scattering properties and scalelengths (i.e. lifetimes). These pronounced variations of $\sum Af$ vs. ρ are accompanied by clear dust color gradients in the 2D maps, unlike the dust color vs. ρ as derived from the spectrum. Since spectroscopic measurements are only obtained in east–west direction and with a very long exposure time, the effect of color variations inside the coma due to disintegrating grains is difficult to detect.

Key words. comets: individual: C/2000WM1 (LINEAR) – comets: general

1. Introduction

The Lincoln Near Earth Asteroid Research (LINEAR) has been proved to be an efficient comet discoverer. The target of this paper, C/2000 WM1, was detected by LINEAR and after determining its orbital parameters, it resulted to be a long period comet with $1/a = 0.000533 \pm 0.000001$ which excludes it from the classical definition of dynamically new in the Oort sense ($a \geq 10^4$ AU) and that has probably made previous passages through the inner solar system (Marsden 2003, private communication). The perihelion took place on Jan. 23, 2002 at $r_H \approx 0.55$ AU, whereas the closest approach to Earth occurred on Dec. 2–4, 2001 at $\Delta \sim 0.32$ AU allowing for high spatial resolution observations (232 km per arcsec).

Before this close Earth approach, the comet was imaged by Szabó et al. (2002) when the it was at $r_h = 2.789$ (on Aug. 22, 2001, i.e. five months prior perihelion). Those images showed a compact circular coma of ~20″ diameter and a thin dust as long as 120″. Some C_2 and CO^+ were also detected, although only an upper limit on the CN abundance could be set at that distance. The level of activity at that heliocentric distance was relatively low with $Af\rho = 275$ cm.

Schleicher et al. (2002) carried out a monitoring of C/2000WM1 in the optical from August 2001 ($r_h = 2.7$ AU) to shortly before perihelion (Jan. 22, $R_H = 0.56$) using the Hall 1.1-m telescope at Lowell Observatory. The photometry and imaging of C/2000 WM1 provided production rates for OH, CN, NH, C_2 and C_3 steadily increasing when the comet approached the Sun. The dust production rate was estimated by means of the $Af\rho$ parameter in the green continuum. From the observations in mid-Nov., the deduced $Af\rho$ was about 1000 cm, to considerably decrease after those dates. This high value might be due to a phase angle effect (very small during Nov.) in such a way that the strong tail is nearly behind the coma and within the photometer's entrance aperture. Furthermore, for the data in Dec., these authors found a strong trend of the $Af\rho$ values with aperture size, decreasing from 460 cm for an aperture radius of 6000 km, to ~300 for $\rho = 20\,000$ km.

Medium resolution spectra were also obtained by Churyumov et al. (2002) on Nov. 22, 2001, allowing the determination of the CN, C_2 and C_3 lifetimes as well as expansion velocities. Possible detection of C_2^- and CO was also reported by these authors.

The observations reported in this paper are part of a wide campaign carried out at ESO in order to fully characterize the gas and dust component of the cometary coma. The planned observations consisted of broadband (R, i) and narrowband imaging and long slit spectroscopy in the visible; broadband (J, H, K), polarimetric and narrow band imaging, and long slit spectroscopy in the near-IR, and broadband and narrowband imaging and spectroscopy in the thermal IR. Unfortunately bad weather conditions prevented observations during almost two of the three (half) awarded nights and the planned program was not completely fulfilled. Moreover the high proper motion of the comet gave problems of tracking during the observational campaign and some images are not appropriate for some detailed studies of the coma morphology. In this paper we present the results derived from the the optical observations, i.e. one single spectrum taken on Dec. 4, 2001, and several series of broadband and narrowband images obtained during Dec. 2 and 4, 2001.

2. Observations and data reduction

2.1. Imaging photometry

Comet C/2000 WM1 (LINEAR) was observed at the European Southern Observatory, La Silla, Chile, preperihelion between December 2nd and 4th, 2001. We used the DFOSC instrument mounted on the 1.5 m Danish telescope (2148 × 2102 pixels, pixel size: 0.″39, FOV 14′ × 13.′4). The first night was photometric, whereas the third one was slightly less transparent, but still appropriate to monitor the comet. On Dec. 3, 2001, bad weather conditions prevented any observations.

Table 1. Properties of broad- and narrow- band filters.

Filter			Molecular band	
ESO #	λ_0 (Å)	$\Delta\lambda$ (Å)	Radical	λ (Å)
452	6488.7	1163.1	Cont.[1] (Bessel R)	
425	7977.9	1428.8	Cont.[1] (Gunn i)	
835	3859.7	50.1	CN	3870
836	4052.3	75.4	C_3	4060
837	4421.6	36.7	cont.	–
838	5110.7	122.8	C_2	5140
840	6838.2	80.9	Cont.	–

[1] Mainly scattered radiation by the dust, although some gas contamination due to C_2 and NH_2 might be present.

The comet was imaged with Bessel R and Gunn i broadband filters, and with narrowband interference filters covering gas (CN, C_2 and C_3) emissions, and others centered in spectral regions known to be nearly free of cometary emission (see Table 1). In each filter, consecutive series of 2 to 5 images were acquired, excepting CN and C_2 that one single image was taken during the observing run. Appropriate bias and flat field frames were also taken each night.

All of the observations were done while tracking on the comet proper motion. Since this proper motion was very high, some of the images present a distorted inner coma and they cannot be used for a detailed study. Details and quality of the imaging observations are presented in Table 2.

For calibration purpouses, standard stars (Area 92 in Landolt 1992) in the Bessel R and Gunn i filters were observed each night. The calibration error resulted to be ~5%. Unfortunately, no standard stars were observed with the narrowband cometary filters. Thus, the CN, C_2, C_3, BC and RC continuum images will be only considered for a morphological analysis of the coma after bias and flat-field correction and sky subtraction. In the case of the BC and RC images, the sky contribution was derived as the number of counts (DNs) needed to obtain a constant Af parameter (A'Hearn et al. 1984) at large cometocentric distances. For the gas emission images, the sky contribution was approximately computed as an average of the measured counts at the edge of the frames.

The position of the comet optocenter in every image (well tracked on the comet nucleus) was determined by fitting a two-dimensional Gaussian to the innermost 20 pixels of the coma with an uncertainty ≤0.7 pixels. All images were recentered using the derived optocenters and the images taken in consecutive series with the same broad- or narrow- band filter were median combined to be further analysed.

Figure 1 shows the gas and dust coma, as imaged with the interferometric cometary filters after bias and flatfield correction, and sky subtraction. Note that gas images have not been

Table 2. Details of the imaging observations.

Date (2001)	Time UT	Band	Δ AU	r_h AU	km per pixel	PA deg.	Phase deg.	#	Image quality
Dec. 2	00:55–01:40	Gunn *i*	0.318	1.213	89.9	62.1	38.6	6	66% bt
	01:45–02:13	Bessel *R*	0.318	1.213	89.9	62.0	38.8	3	75% bt
	02:08–02:33	CN	0.318	1.212	89.9	62.0	38.9	1	gt
	03:16–03:54	C_3	0.318	1.212	89.9	61.9	39.1	2	50% bt
	04:09–04:22	BC	0.318	1.211	89.9	61.8	39.4	2	50% bt
	04:33–04:42	C_2	0.317	1.210	89.7	61.8	39.4	1	bt
	04:48–04:58	RC	0.317	1.210	89.7	61.7	39.5	1	bt
Dec. 4	02:37–03:11	RC	0.318	1.179	89.9	59.8	45.8	2	gt
	03:34–03:43	Bessel *R*	0.318	1.178	89.9	59.7	46.1	7	gt
	03:45–03:52	Gunn *i*	0.318	1.178	89.9	59.7	46.6	3	gt
	04:26–04:45	Bessel *R*	0.318	1.178	89.9	59.7	46.7	2	gt

PA refers to the position angle of the extended Sun-target radius vector. Phase is the Sun-comet-observer angle. r_h and Δ are the heliocentric and geocentric distances of the comet during our observations. # refers to the number of acquired images. bt, gt mean bad and good tracking, respectively.

subtracted from the underlying continuum emission, as it can be clearly seen in the C_2 and C_3 ones.

The median combined frames obtained during photometric nights in the broadband filters were calibrated in Af, i.e. the average albedo ($A(\theta)$, no correction for the phase angle was applied) multiplied by the filling factor (f) that represents the percentage of area covered by the dust (see Tozzi & Licandro 2002). This notation $Af\rho$, introduced by A'Hearn et al. (1984), defines a measurement unit related to the dust production rate of a comet. It can be interpreted as the average of the percentage of solar radiation scattered by the cometary dust toward the observer. In terms of measurable quantities, it is equal to

$$Af = \left(\frac{2\Delta r_h}{\rho}\right)^2 \frac{F_c}{F_S} \quad (1)$$

where Δ and r_h are the comet's geocentric and heliocentric distances, respectively, ρ is the projected radius of aperture, F_c is the measured cometary flux in every filter, and F_S is the solar flux in the same filter.

2.2. Long-slit spectrophotometry

A single spectrum was taken on Dec. 4, 2001 at 04:05 UT with a grating of 300 lines per mm and a slit width, length of 2.″5, >5′, respectively. This resulted in an observable spectral range between 3400 Å and 9300 Å with a wavelength scale of 5 Å per pixel and a spatial scale of 0.″39 per pixel. The slit of the spectrograph was orientated east−west. Given the position angle of the extended Sun–comet radius vector (~60°), the dust profiles will barely lie on the tail direction as projected on the plane of the sky. For absolute calibration, we obtained observations of the spectrophotometric standard star HR718 ($V = 4^m279$) (Hamuy et al. 1992) with a slit width of 5″. The spectra were reduced using the ESO-MIDAS standard reduction context *long* for long-slit spectra. The spectra were bias subtracted, flatfielded, wavelength calibrated (using He−Ne reference spectra), extinction corrected (using the standard extinction curve for La Silla) and finally flux calibrated. Since the spectrum of C/2000WM1 covers the entire length of the slit, it is not possible to extract the sky contamination directly from the spectrum itself. Instead, we attempted to compute the sky flux by extrapolating the comet continuum flux under the assumption of a $1/y$ dependency, with y, being the spatial distance along the slit from the optocenter (or equivalently ρ, projected cometocentric distance). As with the usual sky subtraction techniques, two "sky" regions are chosen, located on either side of the optocenter (i.e. "upper" and "lower") as far away from it as possible, avoiding background spectra. Instead of assuming the flux in these regions to be representative of the sky flux and interpolating for the spatial region "underneath" the comet spectrum, we subdivided each sky region further in two parts. For each sub-part we approximated the cometary continuum flux by fitting a "reddened" solar spectrum to the emission free regions of the cometary flux. Under the assumption that the comet's continuum flux is distributed along the slit as follows: $F_{comet}(y) = y_0/y + F_{sky}$, we can now use the approximated flux in the two sub-regions to solve the equation for our two parameters. First for $y_0 = (F_2 - F_1)\frac{y_1 y_2}{y_1 - y_2}$, which leads us to a value for F_{sky} through the original equation. The distributions for the sky flux computed in this way for the two "sky" regions can now be used to interpolate the sky flux over the entire slit. The so generated 2D sky contribution was subtracted from the cometary spectrum. Our estimate of the error in this sky flux determination is ≤30% over the entire wavelength range.

3. Data analysis

The narrowband images have been mainly used to study the gas and dust coma morphology. The absolute calibration of the

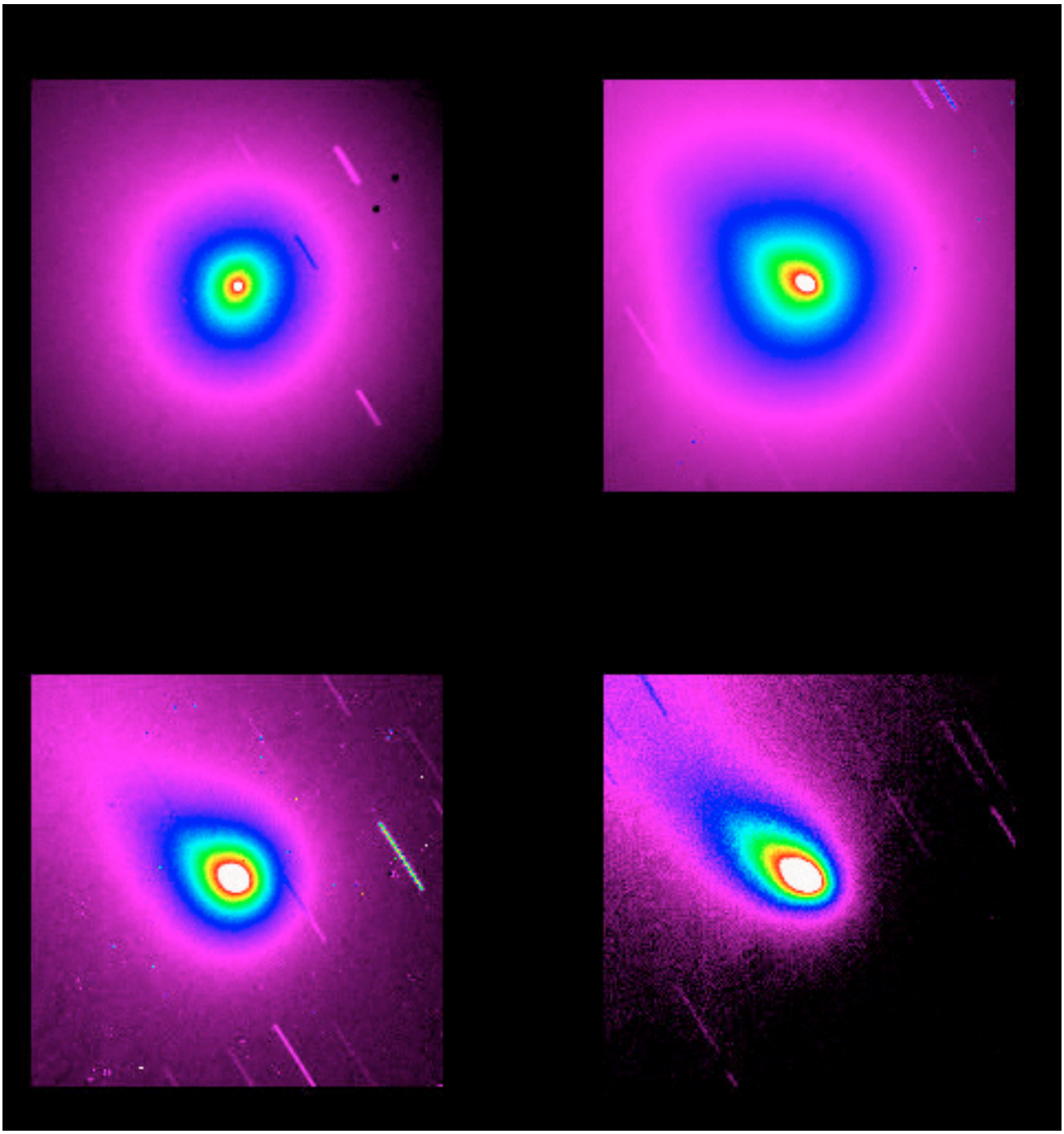

Fig. 1. Images of C/2000 WM1 taken with the interferometric CN, C_2, C_3 and BC filters after bias and flatfield correction, and approximate sky subtraction. North is up and East is to the left. Position angle of the Sun is ~240º as measured from north toward east, whereas the Phase angle is ~60º. The common angular scale is 510 × 510 arcsec, meaning 118 000 × 118 000 km at the comet distance. Note that the CN coma shows a slight asymmetry in the north-south direction. All of the images have been normalised to 1000 DNs as the peak intensity.

broadband images in Bessel *R* and Gunn *i* has provided us with dust production rates (in terms of $Af\rho$) and with the behaviour of the dust and its color as a function of the projected cometocentric distance, ρ. A morphological analysis of the coma has been also carried out from these broadband images.

The study of the spectrum has allowed us the determination of parent and daughter species lifetimes (Festou 1981) and production rates for CN, C_2, NH_2 and C_3. Furthermore, the dust behaviour is analysed from two different spectral regions which are known to be relatively free of gas emission (see Table 3, and Schulz et al. 1994).

3.1. Coma morphology

We have investigated the general spatial distribution of particles in the coma of C/2000 WM1 in the case of CN, C_2 and C_3 as well as in the continuum images (either broadband or narrowband ones).

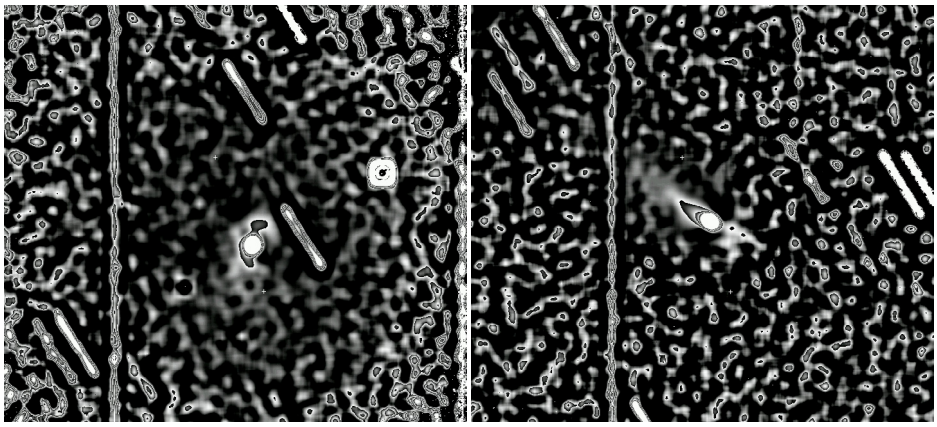

Fig. 2. CN and BC processed images through Laplace filtering. Note than in CN a faint and double-jet structure appears in the approximately north−south direction (11 500 km projected length, mean position angle 340 and 170°), whereas in the blue continuum image a faint, short and narrow sunward structure (∼20 000 km projected length, position angle 230−250°) can be also seen besides the incipient dust tail.

Table 3. Emission and continuum bands extracted from the spectra.

Spectral region (Å)	Species	Left. hand cont. (Å)	Right hand cont. (Å)
3830–3905	CN	3700–3815	3910–3970
3975–4150	C_3	3910–3970	4155–4190
4860–5185	C_2	4780–4850	5195–5295
5673–5766	NH_2	5653–5670	5769–5790
4820–4850	Cont. 1		
5200–5250	Cont. 2		

Two different methods were applied: 1) adaptive Laplace filtering (Richter 1978, 1991; Boehnhardt & Birkle 1994), and 2) radial renormalization (A'Hearn et al. 1986). The former method does not depend on the accuracy of the comet nucleus centering by a 2D Gaussian and it is more sensitive to gradient change on different scales depending on the width of the spatial filtering applied. The latter method uses the azimuthally averaged, radial profile of the coma flux to create a 2-dimensional image of the average coma flux level and divides it through the original image of the comet, enhancing any deviation from spherically symmetric coma.

The results of applying the enhancement techniques to the non-calibrated images acquired with the interferometric filters are as follows: (i) in the continuum images, an ordinary dust coma (rather symmetric with respect to the Sun–comet direction), the incipient dust tail, and a faint, short and narrow sunward structure (∼20 000 km projected length, position angle 230−250°) can be detected; (ii) in CN, a faint and double-jet structure appears in the approximately north-south direction (11 500 km projected length, mean position angle 340 and 170°). Neither a counterpart of the dust structure is seen in the gas emission band filters nor are the double jets with counterparts in the dust band images. Figure 2 shows the coma structures described above as detected in the CN and BC images processed through Laplace filtering.

The feature present in CN is not so clearly seen either in C_2 or C_3 when applying the renormalization technique. However, the only asymmetry seems to be due to the dust tail. This is due to the fact that the C_2 and C_3 interferometric filters contain more light scattered by the dust, i.e. underlying continuum, than the CN filter. To solve this problem, we have tried an approximate 2D continuum subtraction from these images making use of the flux calibrated spectrum and the transmission curves of the C_2, C_3, BC and RC filters. Since the cometary images acquired during Dec. 2, 2001 in C_2, BC and RC are affected by bad tracking (clearly reflected in the distorted coma appearance and in the discontinuous star trails), this 2D subtraction produces artifacts in the inner coma, specially in and around the optocenter, hampering our effort to obtain a reliable enhanced feature. Because of this problem, we applied technique 1 (i.e. adaptive Laplacian filtering, not dependent on the nucleus centering) to the C_2 and C_3 resulting into a structure most likely due to the continuum emission from the dust contamination of the interferometric filters since it falls exactly at the same position as the incipient dust tail is located. Thus, if any C_2 and/or C_3 structure exists, the gas overabundance in the region containing any structure has to account less than 10% the isotropic coma to be smeared out by the dust contribution.

Nevertheless, by converting the cartesian coordinates images into polar coordinates, and analysing the intensity vs. the azimuthal angle, any deviation of a spherically symmetric emission can be detected. By doing so, we found out that although the C_2 and C_3 have a considerable dust contamination, a slight asymmetry at the same angles as the one in CN were present. A very rough estimate of the dust contamination of the C_2 and C_3 filters was done by studying the behaviour of the integrated DNs in an annulus of radius ρ vs. ρ, and comparing this integral with that obtained from the images acquired in the blue and red continuum. The pure emission from a daughter species presents an increasing integral at short cometocentric distances, reaching a broad maximum at certain distance and then it steadily decreases at long ρ. On the other hand, that integral for the dust component shows a steep increase in the inner coma to become constant at large distances. Comparison of both behaviours in the inner coma, i.e. for dust

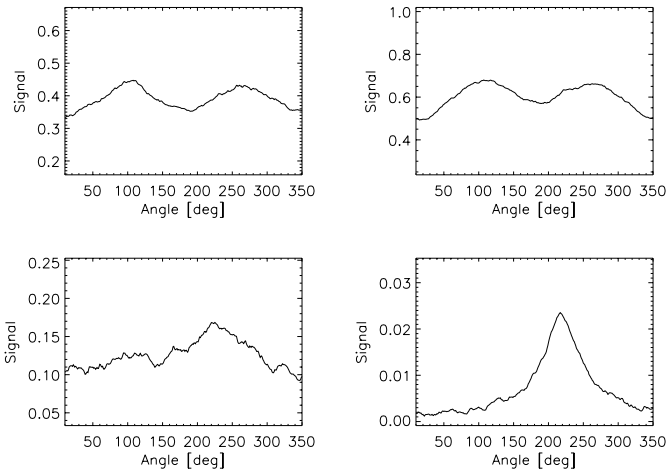

Fig. 3. Azimuthal distribution of material for CN, C_2, C_3 and blue continuum from top left to down bottom. The profiles have been obtained by averaging the emission in an annulus 3000 km wide centered at 45 000 km from the optocenter. West corresponds to $\Phi = 0°$ and South to $\Phi = 90°$. Note that at $\Phi \sim 110°$, 275° (or 160° and 355° as measured from North towards East) there is an overabundance of CN and C_2, not detected in C_3. The enhanced emission at $\Phi \sim 215°$ (or ∼55° from North toward East) in the blue continuum panel exactly coincides with the location of an incipient dust tail.

and gas+dust, allows us to guess the contribution of the continuum emission to the gas interferometric filters. According to this, the blue continuum image (less affected by bad tracking) was multiplied by a certain factor (obtained from the previous comparison) and subtracted from the C_2 and C_3 images. This approximate procedure provided us with gas images relatively free of dust contamination. The so obtained "pure" gas images were again converted to polar coordinates and the results are shown in Fig. 3 together with that for CN and for the blue continuum. It can be clearly seen that the C_2 abundance is enhanced at two angles, coinciding with the CN ones, and at a definitely different position of the dust tail. The case of the C_3, due to the lower S/N, did not produce as satisfactory results as for C_2. Thus, any coma asymmetry in C_3 cannot undoubtedly be claimed.

3.2. Spatial profiles

3.2.1. Spectrophotometric observations

The spectrum taken on Dec. 4 was used to investigate the CN, C_2, NH_2 and C_3, and continuum profiles in east−west direction.

The spectral regions are specified in Table 3. For the subtraction of the underlying continuum in the gas emission bands, we have measured the continuum bordering each emission band (see Table 3) and approximated the continuum contribution to the band by interpolating the left-hand and right-hand continua.

The conversion of the emission band fluxes into column densities was done with a constant g-factor for C_2 and C_3 (A'Hearn et al. 1995), whereas the CN g-factors were calculated for the heliocentric distance and velocity of C/2000 WM1 on December 4, 2001, from the set of values given by (Schleicher 1983). In the case of NH_2, we used the g-factor in Tegler & Wyckoff (1989) divided by two to account for the fact that the even bands and the odd bands only populate half of the NH_2 molecules in the ground state (Arpigny 1994).

Two different continuum regions were extracted from the spectra which are known to represent relative clean continuum (Schulz et al. 1994). The flux calibrated continuum profiles were multiplied by $2\pi\Delta^2$ and r_h^2 and normalized to a unit area of 1 km^2 at the position of the comet. This leads to a surface brightness in erg s^{-1} km^{-2} Å^{-1}, which is independent of the geocentric distance as well as of the size of the aperture, and normalized to the solar flux at $r_h = 1$ AU. It therefore, allows a direct comparison of the day-to-day variations in the continuum profiles.

The Vectorial modeling (Festou 1981) was used to derive parent and daughter lifetimes (τ_p, τ_d) for the gas species previously mentioned. To derive the τ_p and τ_d that better resemble the shape of the observed profiles, we constructed theoretical CN, C_2, NH_2 and C_3 radial profiles with an arbitrary (however approximated) gas production rate with lifetimes spanning the reported values (Schulz et al. 1991, 1993; Huebner et al. 1992; Huebner & Link 1999). Parent species velocities were computed as $v_p = 0.85 \times r_h^{-0.5}$ (Biver et al. 1999, 2000), whereas daughter ones were held constant and equal to $v_d = 1.0$ km s^{-1} except for CN having $v_d = 1.19$ km s^{-1} (Bockelée-Morvan & Crovisier 1985).

Once the theoretical profile was computed, we compared it with the observed profile by dividing both profiles. We selected the pairs (τ_p, τ_d) giving rise to those theoretical profiles which standard deviation of the quotient calculated at distances $3 < \log\rho < 4.2$ (i.e. between 1×10^3 and 1.6×10^4 km not to hit the sky values) was lowest. Table 4 contains the (τ_p, τ_d) that give rise to theoretical profiles best reproducing the observed ones. The gas production rates were obtained once the lifetimes were derived.

The so obtained parameters, i.e. parent and daughter lifetimes, for the C_2 profile are unrealistically high (80 000 and 215 000 s) since the inner part of the observed profile is very flat and this flatness can be only reproduced by a long parent lifetime in a two-steps photolytic model. Such a flattening of the C_2 profile has been observed previously (Tozzi & Festou 1990; Schulz et al. 1993) and is expected on theoretical grounds (Huebner & Keady 1983). To artificially compensate for this effect and to nicely fit the whole profile with "usual" lifetimes ($\tau_p = 37\,000$ and $\tau_d = 100\,000$ s), the C_2 production rate in the vectorial model has to be decreased for about the preceding 0.2 days before the observation was taken. Let us note that the C_2 steady state production rate, by making use of the previous parent and daughter lifetimes, listed in Table 4, more realistically represents the C_2 activity of comet C/2000 WM1 although the artificial profiles generated by the two-steps photolytic model nicely fit the observations. Figure 4 displays the result of the theoretical column density profiles obtained with parameters listed in Table 4 together with the observed ones.

Previous gas production rates for comet C/2000WM1 (Szabó et al. 2002; Schleicher et al. 2002) were derived by means of the Haser model with parameters listed in

Table 4. Lifetimes and production rates as derived from the Vectorial modeling. Gas production rates derived from the Haser modeling with customary scale lengths.

Species	τ_p	τ_d	Q_{Fes}	Q_{Has} [a]
	($\times 10^4$ km)	($\times 10^5$ km)	($\times 10^{25}$ s^{-1})	($\times 10^{25}$ s^{-1})
NH_2	0.7	0.74	21.5	24.9
CN	3.9	3.9	24.3	15.2
C_2	3.7	1.0	42.5 ($\Delta t_1 \rightarrow \infty$)	
			20.0 ($\Delta t_2 \rightarrow 0.2$ days)	
	3.7	1.0	31.1[b]	31.8
C_3	0.15	1.0	0.36	0.50

[a] Haser modeling assumes $v_p = v_d = 1$ km s^{-1}.
[b] Steady state Vectorial modeling.

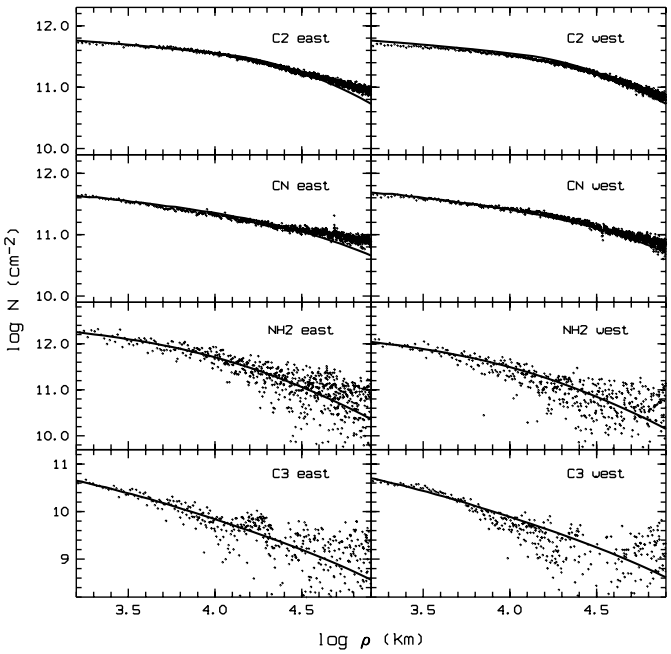

Fig. 4. C_2, CN, NH_2 and C_3 column density profiles of Comet C/2000 WM1 (dots) in the east−west direction. The solid lines represent the theoretical profiles obtained by means of the Vectorial modeling with lifetimes and production rates listed in Table 4.

A'Hearn et al. (1995). In order to consistently compare our results with previous published ones, we have also computed the gas production rates means of that formalism and the results are included in Table 4.

From the fully reduced and calibrated spectrum (in erg s^{-1} km^{-2} Å^{-1}) we have derived log B vs. log ρ profiles in east and west direction. Given the PA (=60°), these profiles do not lie on tail direction where most of the cometary dust is located. These profiles follow the law log $B \sim -m \log \rho$ in east−west direction, and the slope m of the linear fits shown in Fig. 5 is listed in Table 5. The standard deviations of these fits is ∼0.02.

Estimates of the production of the dust in comets are usually made by means of the parameter $A(\theta)f\rho$ (A'Hearn et al. 1984). From the radial continuum flux in the east−west

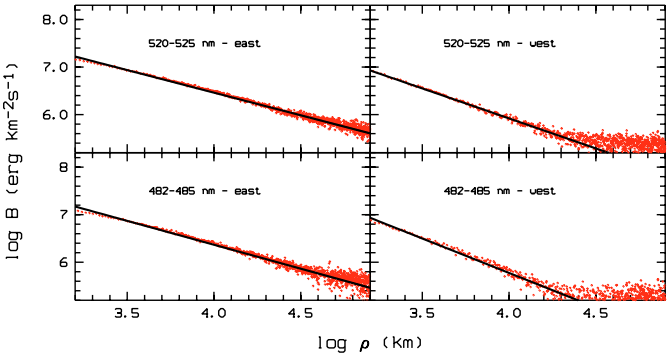

Fig. 5. Linear fits of the dust brightness profiles in log – log representation.

Table 5. Linear fits to log B vs. log ρ in two selected continuum regions and for the inner and outer dust coma in east and west direction.

Region	log $\rho \geq 3.2$		$Af\rho$ (cm)	log $\frac{Q(C_2)}{Af\rho}$	log $\frac{M_{gas}}{M_{dust}}$
	East	West			
Cont. 1	1.05	1.56	350		
Cont. 2	0.98	1.27	310	24.01	0.80

direction, we computed $Af\rho$ for different apertures. This parameter was found to considerably vary as a function of ρ regardless the continuum region (either cont1 or cont2 in Table 3 or an additional 680−690 nm band). In the case of the two continua listed in Table 3, we obtain an $Af\rho$ parameter in the order of 300 cm at large apertures ($\rho \geq 30\,000$) km. The quotient of the C_2 production rate and the dust production rate (parameterised by $Af\rho$), as indicative of the gas or dust enrichment, is listed in Table 5.

If CN is produced in constant proportion to OH (Schleicher et al. 1987), the Q(CN)/$Af\rho$ quantity is proportional to Q(OH)/$Af\rho$ and therefore, the gas-to-dust mass ratio can be determined. Since the long-slit spectra do not cover the OH emission in the UV, we have used the CN observations and the mean ratio of OH to CN, log (Q(OH)/Q(CN)) = 2.5 (A'Hearn et al. 1995), to derive the OH production rate (typical values for log (Q(OH)/Q(CN) range from 2.83 to 2.17, which implies that the OH derived from this expression can reasonably be as much as 2 times smaller or larger than the actual value). In line with A'Hearn et al. (1995), the gas-to-dust mass ratio can be evaluated by

$$\log\left(\frac{M_{gas}}{M_{dust}}\right) = \log[Q(OH)/Af\rho] - 25.4. \quad (2)$$

According to this expression and using the Q_{CN} obtained with the Haser model (see Table 4), we computed a gas-to-dust mass ratio of ∼6.3 at r_h = 1.178 AU (with an error of a factor of ∼2, introduced by the approximate Q_{OH}).

3.2.2. Broadband imaging

For the analysis of the spatial dust profiles, besides the continuum regions in Table 3, we also considered the images taken in the Bessel R and Gunn i broadband filters (see Table 1)

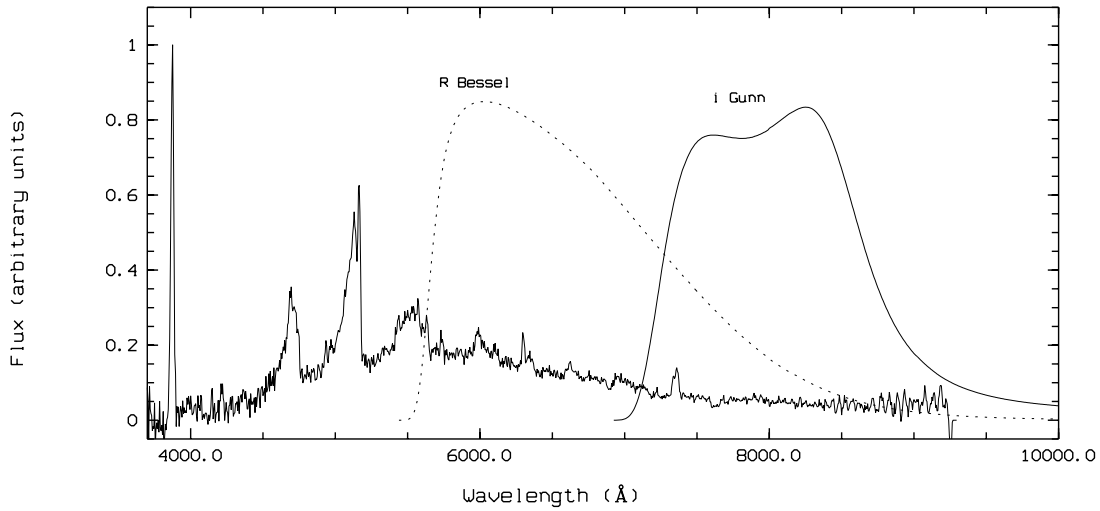

Fig. 6. Transmission curves of the broad band filters (*R* Bessel and *i* Gunn) superimposed on an spatially averaged spectrum of C/2000 WM1 and normalised to the maximum CN emission. Both broad band filters, beside the continuum emission, also cover the $\nu'_2 = 6,\ 7,\ 8$ and 9 NH_2 and $\Delta\nu = -2,\ -3$ C_2 bands.

which contain 2D information about the dust distribution in the comet as projected on the plane of the sky. These filters might still contain some gas contamination from several C_2 and NH_2 bands as seen from Fig. 6, where the transmission curves for both filters are superimposed onto the spatially averaged and normalised cometary spectrum.

The study of the images, calibrated in the $Af\rho$ frame (A'Hearn et al. 1984), provides us with values of this parameter as a function of the projected cometocentric distance. Additionally, the dust activity is also quantified by the gradient of the integral of the Af parameter ($\sum Af$) measured in a circular aperture as function of ρ. Figure 7 shows the values of $Af\rho$ and $\sum Af$ as obtained from imaging the comet in Bessel *R* and Gunn *i*. A peculiar behaviour, for both parameters regardless the spectral band, is seen. More concise, $\sum Af$ sharply increases at $\rho \leq 12\,000$ km. To investigate whether this feature is due to the non-quantifiable gas contamination of the broadband filters, we applied the same procedure to the non-calibrated continuum images taken with the ESO#837 and #840 interferometric filters. Note that the resulting profiles are not dependent on flux calibration. A completely similar behaviour is detected: sharp increase of $\sum Af$ at $\rho \leq 12\,000$ km. Additionally, $Af\rho$ and $\sum Af$ vs. ρ derived from the near-IR images in the *J*, *H*, *K* band also exhibit the same behaviour (Tozzi et al. 2002)

For a dust coma represented by the simple outflow model (i.e. neither vaporization of ice particles nor dust fragmentation) with constant expansion velocity and no short time scale variation of dust production rate, these quantities should be constant with ρ. The fact that noticeable variations do happen can be explained if the size and/or composition of the dust grain population is changing and if a sudden change of cometary activity occurs. More concise, these profiles are very steep in the inner coma. This steepness cannot be due to a dramatic change of activity since the same profile is seen on every night, during the observations run, either in the optical or in the IR range (see Tozzi et al. 2002). Since the parameter $\sum Af$ is proportional to

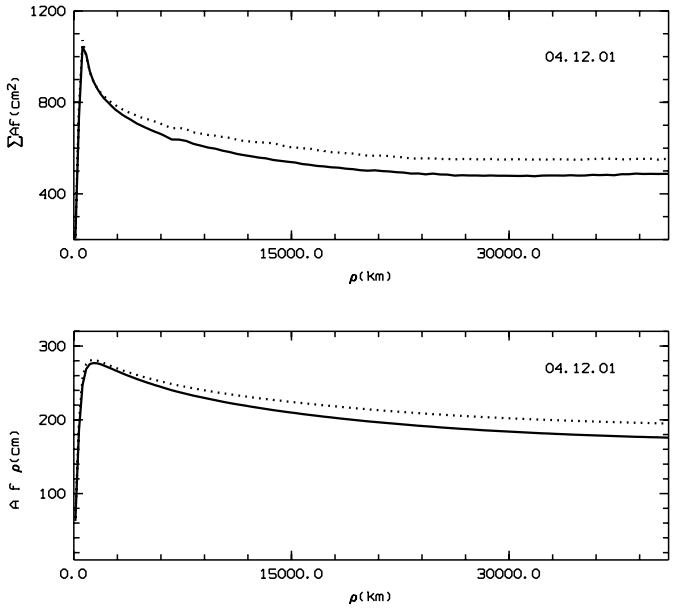

Fig. 7. $Af\rho$ and $\sum Af$ as a function of ρ for images taken in the *R* Bessel (solid line), and in the Gunn *i* (dotted line) filters.

the dust grains column density at a nucleocentric distance ρ, the shape of this profile (see Fig. 7) indicates that a fraction of the solid component of the coma is destroyed while traveling outward. The profiles are very well fitted with a constant value for $\sum Af$ as representative of the dust coma at large cometocentric distances, I_0, plus two exponential functions, that is

$$\sum Af(\rho) = I_0 + I_1 e^{-\rho/L_1} + I_2 e^{-\rho/L_2} \quad (3)$$

where L_1 and L_2 can be viewed as "characteristic scale lengths" for the dust. Tozzi et al. (2004) have extended this study to the near-IR images and a complete and extensive analysis of the dust component, in the range 0.6−2.5 μm, is presented there. Let us note that any value of L_1 and L_2 derived from our fits can be inaccurate due to the gas contamination of the *R* Bessel

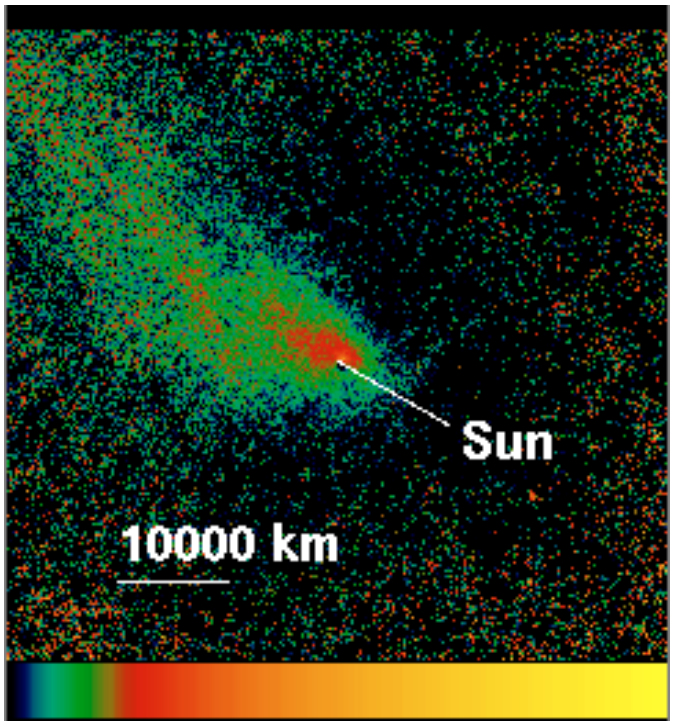

Fig. 8. Dust color map of C/2000 WM1 on Dec. 4, 2001, obtained from the quotient of the calibrated images in Gunn i and R Bessel. The comet nucleus is at the center of the frame which has a full scale of 60 000 × 60 000 km. The look-up table is logarithmic. The panel color scale is such that differences in dust color as much as 35% can be seen.

and i Gunn filters (see Fig. 6). For the purpouse of deriving the dust "scale lengths", the non-calibrated blue and red continuum images can be considered too and they are in the same range as those obtained from the near-IR. The derived scale-lengths seem to indicate that two different populations of dust grains coexist in the coma of C/2000 WM1, one of them having a much shorter "lifetime" than the other and with optical characteristics clearly differentiated from the other.

Prompted by the previous result, we searched for structures in the color maps obtained by dividing the i and R calibrated images. Unfortunately, some of the images obtained in the photometric night (Dec. 2, 2001) are severely affected by bad tracking. Only data acquired on Dec. 4, 2001 can be used to compute two-dimensional dust color maps as the one in Fig. 8. An obvious color gradient with ρ is found in anti-Sun direction. Mean values of the dust color on Dec. 4, 2001 obtained as $Af\rho_i/Af\rho_R$ can be seen in Fig. 9. Dust color is constant beyond ~10 000 km, whereas at shorter cometocentric distances clear variations, correlated with that in Fig. 8, can be seen. A more detailed analysis of the color of the two dust components found in the coma of C/2000 WM1 can be seen in Tozzi et al. (2004).

Bonev & Jockers (2002) also found a peculiar behaviour of the dust coma of comet C/2000 WM1. Whilst the mean reddening was 15%, its spatial distribution was different in the different spectral ranges. It was almost homogeneous in the range 526−713 nm, whereas a strong decrease of the reddening was observed in the range 713−853 nm with decreasing distance to the nucleus. These authors interpreted the observed features as a consequence of the combined influence of the size dependent light scattering properties of the dust particles, their motion under the influence of the solar radiation, and of the variations of the particle size distribution function in the relevant spectral range.

The color of the dust was also investigated from the long-slit spectrum which covers a wide wavelength range and it contains spatial information in the east−west direction. The bandpasses representing continuum emissions were carefully selected since several gas emissions (the NH_2 ν'_2 = 5, 6, 7, 8 and, and C_2 $\Delta\nu$ = −2, − 3 bands) are clearly detected (Fig. 6). The spectral regions used for color computations are: 4390−4500, 4780−4830, 5220−5300, 6800−6900 and 8250−8500 Å. The contribution of the 2nd order of 4125−4250 Å (red part of the C_3 emission band) to the 8250−8500 Å is negligible (≤0.5%) and the intensity in that spectral region mainly arises from the solar light scattered by the dust. The optical spectrum of Dec. 4 was used to compute the reflectivity, $S(\lambda) = F_\lambda/F_\lambda(\mathrm{Sun})$, of cometary dust as a function of ρ.

Normalized reflectivity provides a convenient measure of the grain color, and S' is sometimes referred as the "continuum color". Considering reflectivities at two different wavelengths, the normalized reflectivity is computed by

$$S' = \frac{2}{S_1 + S_2}\left(\frac{S_2 - S_1}{\lambda_2 - \lambda_1}\right) \quad (4)$$

where $\lambda_{1,2}$ represents different combinations of the continuum bandpasses listed above with $\lambda_2 > \lambda_1$. Results for $\lambda_1 = 4805 \pm 25$ Å and $\lambda_2 = 8375 \pm 125$ Å can be seen in Fig. 11. Apart from a clear discontinuity around the optocenter, the cometary dust has a uniform normalised reflectivity of ~−10%/1000 Å in the east−west direction.

For further investigation, we performed east−west, north-south and Sun−tail cuts 2.″5 width on the two-dimensional color map of Fig. 8. The resulting radial profiles are shown in Fig. 10) where we can see that at $\rho \leq 10\,000$ km, the dust color can be regarded as the same in Sun, west and north direction, whereas in east and tail direction the dust color coincides, being slightly redder than in the other directions. Regarding the south direction, no noticeable variations, as compared with the north one, can be seen.

Color (or normalised reflectivity) variations have been found from long-slit spectroscopic measurements as it was the case for Comet Tabur C/1996 Q1 by Turner & Smith (1999) and Lara et al. (2001). The continuum light scattered from the dust in the coma of comet Tabur is bluest at $\rho \sim 1800$ km east photocenter (i.e. Sun direction), whereas westward the reflectivity of the dust was considered as constant at every ρ. The observing geometry and peculiarities of the comet activity were extremely favourable to detect any abnormal behaviour of the cometary dust: (i) the PA of the extended Sun–comet vector was 87° (i.e. east−west direction where the slit was positioned) and (ii) the Sun illuminated hemisphere was considerably more active. Kolokolova et al. (2001) concluded that the dust grains changed their size as well as their composition (evaporation of

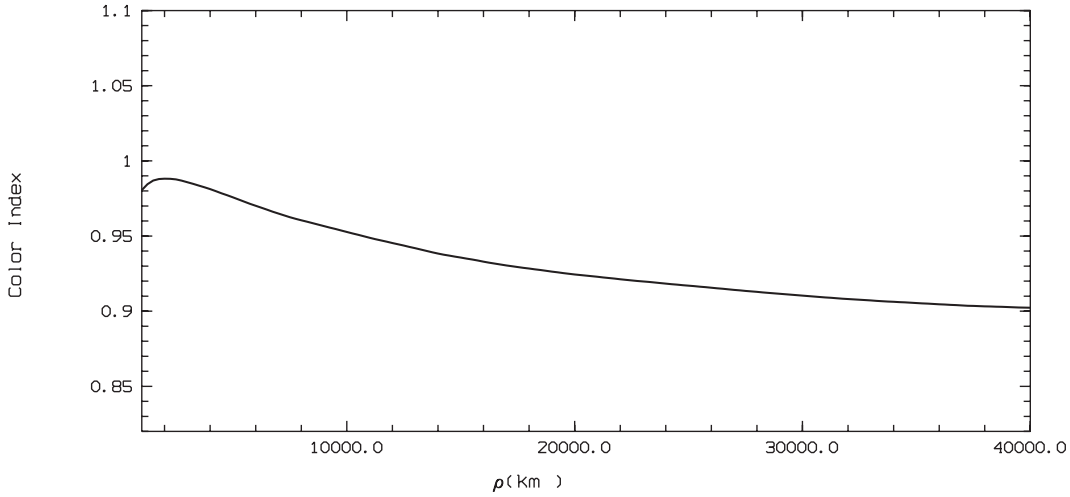

Fig. 9. Averaged dust color of C/2000 WM1 on Dec. 4, 2001 vs. cometocentric distance, ρ, as obtained from the quotient of $Af\rho$ derived from Gunn *i* and *R* Bessel images.

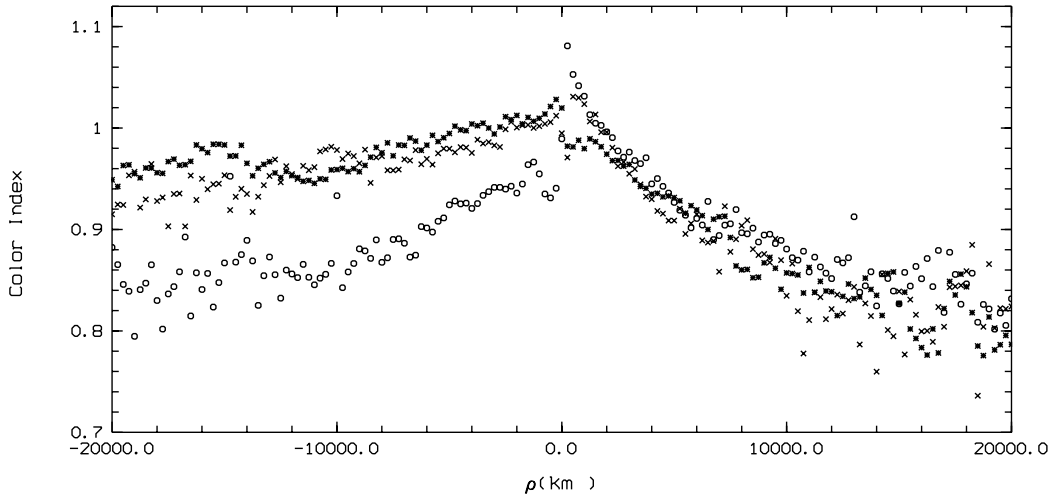

Fig. 10. Dust color variations along several directions as obtained from cuts in the two-dimensional color map (i.e. quotient of the calibrated in Af broadband images). Crosses refer to east ($\rho < 0$)–west ($\rho > 0$) direction. Open circles refer to north ($\rho > 0$)–south ($\rho < 0$) direction. Stars correspond to Sun ($\rho > 0$)–tail ($\rho < 0$) direction.

icy or organic grains or sublimation of icy mantles from silicate cores).

Since the variations of $Af\rho$ vs. ρ in the optical and near-IR images (Tozzi et al. 2004) are noticeable and larger than calibration uncertainties, we believe that the fact that spectroscopic measurements do not reflect any dust color variation as a function of the cometocentric is due to the intrinsic nature of these observations: data only acquired in a single direction (i.e. east−west, which also seems featureless from the 2D color maps), and very long exposure time.

4. Discussion

The analysis of CCD images in several spectral ranges and of long-slit spectra of comet C/2000 WM1 have provided the morphological and compositional information on its coma at perigee.

The dust continuum images show a short sunward jet-like dust structure without clear counterpart in the gas emission bands. Results from own Finson-Probstein calculations for the dust coma and tail of C/2000 WM1 suggest that this feature contains sunward emitted dust from recent nuclear activity, and it appears to be unrelated with the dust observed earlier in the anti-tail of this comet (Watanabe J. 2001). The C_2 gas filter images do not show a similar jet feature, however, a very broad and diffuse enhancement of the flux in the sunward coma hemisphere is noticeable. Gas jets driving the embedded dust jets are known to be wider and more diffuse, a phenomenon that can mimic the absence of gas activity for an observed dust coma feature. The morphological analysis of the CN and C_2 images revealed a double jet in the north-south direction as projected on the plane of the sky, with no counterparts neither in the dust and nor likely in the C_3. Both jets could represent emission from one or two active regions on the nucleus. The presence of gas structures are not always accompanied by the same features in the dust, and this phenomenon is sometimes non-correlated and independent (i.e. Comet Halley, A'Hearn et al. 1986; Larson et al. 1987; Cosmovici et al. 1988; Schulz 1991;

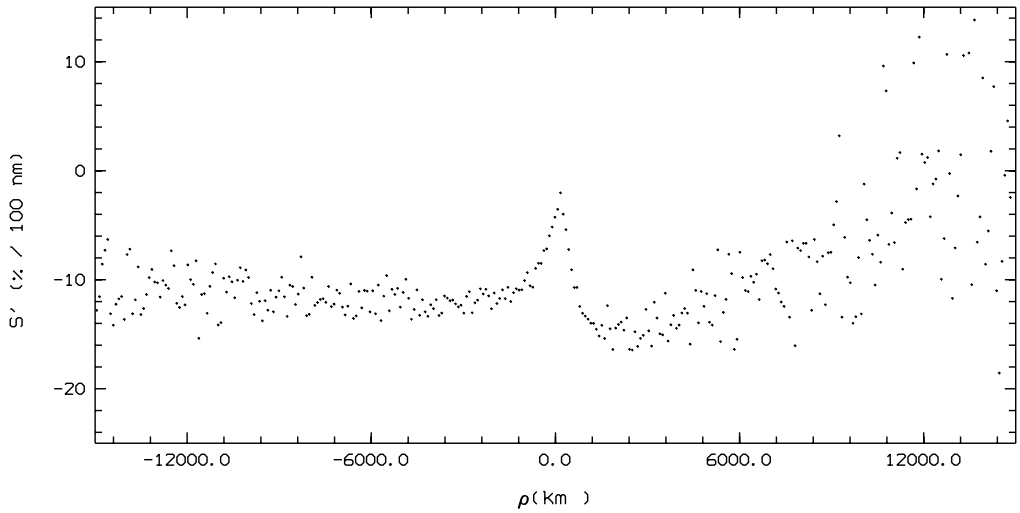

Fig. 11. Dust color in units of percent change in reflectivity per 100 nm vs. cometocentric distance in east (*left*)–west(*right*) direction. The wavelength regions between which the continuum slope was measured are 478−483 and 825−850 nm.

or C/1995 O1 (Hale-Bopp), Schulz et al. 2000; or C/1996 Q1 (Tabur), Lara et al. 2001).

The double gas jet in our CN images can also be interpretated as an arclet phenomenon from a recent splitting event of the nucleus (see Boehnhardt 2002). In this case, the gas jets would represent the collision zone of the coma gases emitted by the mother and daughter fragment(s). The symmetric appearance of the jets, the orientation perpendicular to the Sun–comet line and the absence of dust counterparts are typical attributes seen in arclets of splitting events. Also the viewing geometry from Earth (around quadrature to the Sun) can be considered favourable for the arclet detectibility. However, no fragment was detected in our images nor are they reported for C/2000 WM1 in general. On the other side, unexpected brightening of the comet is reported for the period of our observations (and shortly after perihelion passage).

Theoretical predictions of the photodissociation time scales for many cometary species under solar irradiance have been provided by Huebner et al. (1992) and Huebner & Link (1999). Solar photo rate coefficients and excess energies for dissociation and ionization are calculated both for low and high solar activity. According to Huebner & Link (1999), the lifetimes for HCN and CN at 1 AU amount to 7.94×10^4 s and 3.15×10^5 s at low solar activity, and to 3.19×10^4 s and 1.34×10^5 s at high solar activity. Bockelée-Morvan & Crovisier (1985) reported the HCN photodissociation rate of the order of 1.5×10^{-5} s^{-1}, i.e. lifetime $\sim6.7\times10^4$ s. Note that the solar activity was at its maximum during 2001. From our analysis of the CN profiles, the parent lifetime we obtain, 3.9×10^4 s, agrees reasonably well for HCN as the sole precursor of CN in comet C/2000 WM1. On the other hand, the deduced CN lifetime, 3.9×10^5 s is too large when compared to the values reported by Huebner & Link (1999) for the same high solar activity. The deduced valued is more appropriate for a low solar activity, although still within ranges given by Jonhson et al. (1984) for 1P/Halley. Making use of the derived lifetimes and the Vectorial modeling, the CN production rate on Dec. 4 is 2.43×10^{26} s^{-1}, whereas the Haser modeling provides a (widely known) slightly lower production rate of 1.52×10^{26} s^{-1}. Our result is above the value that an interpolation in Fig. 1 of Schleicher et al. (2002) for $\log r_h \sim 0.071$ ($r_h \sim 1.178$) would give rise. Assuming that CN is solely produced by HCN photodissociation (as the CN parent lifetime seems to indicate) with a quantum yield of 1, the $Q_{HCN}/Q_{H_2O} \sim 0.28\%$, close to the maximum ratio given in Biver et al. (2002) derived from simultaneous millimeter/submillimeter observations of water and hydrogen cyanide production rate in 24 comets, 13 of them being long-period ones.

The fit of the C_2 column density profiles requires the decrease of the gas production rate with time in the vectorial model as a step-like function to decrease the C_2 abundance in the inner coma profile. Flat shape C_2 profiles have been already observed in other comets (see Tozzi & Festou 1990; Fink et al. 1991; Schulz et al. 1993) and they were interpreted as due to the presence of a halo of large icy particles, or due to CHON grain halo (Fink et al. 1991). The fact that the multi-wavelength range analysis of the continuum emission shows the existence of two dust components disintegrating in the coma strengths this scenario for the case of C/2000 WM1. The sublimating icy particles might be a non unimportant source of the observed C_2 and the responsible for the extreme flatness of the profiles, together with the fact that this species is thought to be a granddaughter one. Any of the suggested models leads to an increased C_2 production further away from the nucleus as it is simulated by the temporally altered C_2 production rate in the vectorial model. Also, chemical models of the coma indicate that C_2 is formed primarily by chemical reactions and that its density distribution considerably deviates from a Haser model (Huebner 1981). The production rates derived from the Haser modeling (3.18×10^{26} s^{-1}) or from a steady state Vectorial modeling (3.11×10^{26} s^{-1}), although not reproducing the observations in the inner part of the coma, are more realistic than that obtained from a two-steps photolytic model. These two values are slightly larger than the value computed at the heliocentric distance of our observations from an interpolation of the data in Fig. 1 of Schleicher et al.'s (2002)

paper. C_2 was detected by Szabó et al. (2002) when the comet was at 2.89 AU heliocentric distance. The total luminosity, integrated in an aperture of 10 500 km, was 6.3×10^{15} erg s^{-1}, meaning $Q_{C_2} = 5.13 \times 10^{24}$ s^{-1}. By considering this value, the ones reported by Schleicher (2002) and the one presented in this work, the C_2 production rate has varied as r_h^a with $a \sim -2.5$.

Lifetimes for C_3 and its unknown parent species presented in this work are within reported values for other cometary observations and determined by Krasnopolsky (1991) from TKS-Vega measurements. Unlike the cases of CN and C_2, the C_3 production rate derived in this work seems to be lower than the one presented in Schleicher et al. (2002) by a factor of 2, still bracketed by model uncertainties.

Since the process $NH_3 + h\nu \rightarrow NH_2$ is the responsible for most of the observed cometary NH_2 (Huebner & Link 1999), ammonia production rate is 2.49×10^{26} s^{-1} with usual parent and daughter lifetimes. The few direct evidences of ammonia are a single detection of the 1.25 cm (3, 3) line toward Comet IRAS-Araki-Alcock (C/1983 H1) by Altenhoff et al. (1983), the in situ measurements of the peaks near mass 17 with the Giotto spacecraft ion mass spectrometer (IMS) and neutral mass spectrometer (NMS) for 1P/Halley, and the detection of the (1, 1) and the (3, 3) transitions of NH_3 in Comet 1996/B2 (Hyakutake) by Palmer et al. (1996). Since 100% efficiency in the process $NH_3 + h\nu \rightarrow NH_2 + H$, the ammonia abundance, relative to H_2O, in C/2000 WM1 is 0.2−0.5%, where $Q(H_2O)$ has been taken from Schleicher et al. (2002). This ammonia-to-water ratio is in accordance with the Q_{NH_3}/Q_{H_2O} reported for other Halley family and long-period comets, either old or dynamically new (see Feldman et al. 1993), placing the ratio between 0.4% and 0.8%, and more recently for Comet Hyakutake (0.3%) derived by Palmer et al. (1996).

From the data in Fig. 1 in Schleicher et al. (2002) and in Table 4 of Szabó et al. (2002), the gas-to-dust ratio ($\log \frac{Q_{C_2}}{Af\rho}$) seems not to have dramatically changed from Aug. 2001 to Jan. 2002, increasing from ∼22 at $r_h \sim 2.25$ AU to ∼23.5 at shorter heliocentric distances ($r_h \sim 1.1$−1.2 AU). For the same $r_h = 1.178$, our results point to a slightly higher gas-to-dust ratio of 24.1. As Schleicher et al. (2002) and Schleicher (2003, private communication) have pointed out, the dust production rates ratios during October and November 2001 might be unrealistically high, decreasing the gas-to-dust ratio. The phase angle varied between 21° and 26° from August to October, decreased to 15° during November, and reached 72° in December. Therefore, enhanced backscattering at small phase angle contributes to high values in November near 1 AU together with a strong tail that lies behind the coma and thus, partially within the photometer's entrance apertures. These high $Af\rho$'s lower down the gas-to-dust ratios. Similarly, the $\frac{M_{gas}}{M_{dust}}$ reported from previous observations (∼3, with large uncertainty due to the phase angle effect in the determination of $Af\rho$) and ours (∼6) is in the same order of magnitude, bearing in mind that our determination is affected by an uncertainty of a factor about 2 due to a non-simultaneous observation of the OH emission.

From a general point of view, the gas coma composition of C/2000 WM1, in terms of relative abundance of species and gas-to-dust ratio, can be considered as typical for long-period comets. At $r_h = 1.178$ AU pre-perihelion, $\log (C_3/CN) \sim -1.48$, $\log (Af\rho/CN) \sim -24.00$, gas-to-dust mas ratio of about 6, and $\log (C_2/CN) \sim 0.32$, that is C/2000 WM1 presents an enrichment in carbon-chain species. This characteristic has been frequently reported in long-period comets (see database in A'Hearn et al. 1995; Biver et al. 2002) that were formed in the Uranus-Neptune region of the protoplanetary nebula and subsequently ejected into the Oort cloud.

Unlike the usual behaviour of the gas composition of C/2000 WM1, the dust shows intriguing aspects. The functions $\sum Af$ and $Af\rho$ versus ρ, regardless the wavelength range (Lara et al. 2002; Tozzi et al. 2002), differs from that expected for long-lived grains produced at a steady rate and outflowing at constant velocity. These peculiarities, which need detailed investigation and modeling, are presented elsewhere (Tozzi et al. 2004).

5. Conclusions

From the analysis of optical imaging and long-slit spectroscopy, the gas and dust of comet C/2000 WM1 has been characterised.

The gas coma shows a double jet in CN and C_2 pointing perpendicularly to the Sun–comet direction, as projected on the plane of the sky. The presence of the any structure in C_3 cannot be ascertained with the available data.Furthermore, the C_2 gas filter images also displays a very broad and diffuse enhancement of flux in the sunward coma hemisphere. These gas jets and hemispheric asymmetries have no counterparts in the dust, phenomenon which seems not to be unrare as it has been detected in several other comets. On the other hand, besides the dust tail in a position angle of ∼60° the dust coma shows a faint, short and narrow sunward structure. This feature contains sunward emitted dust from recent nuclear activity.

The dust brightness profiles in the east−west direction can be linearly fitted, in a double logarithmic representation, that is, $\log B \sim -m \log \rho$ with $m = 1.21 \pm 0.26$. Similarly, the brightness profiles derived from an azimuthal averaging of the R and i images do also strictly follow the law $\log B \sim (-1.10 \pm 0.06) \log \rho$. This behaviour, which in principle seems to fulfill the conditions a steady-state dust coma, is disturbed when the calibration (in the $Af\rho$ frame) of the R Bessel and i Gunn images is done. The $Af\rho$ parameter and $\sum Af$ present a steep decrease at $700 \leq \rho < 15\,000$ km that can be interpreted as a dust coma composed in its inner part of two different populations of grains with clearly different physico-chemical properties. Furthermore, the dust color maps also reveal that a color gradient exists at $\rho \leq 16\,000$ km.

Acknowledgements. This work was based on observations obtained at ESO La Silla within programme No 68.C-0506(C). The research carried out has been partially supported by the Spanish Ministerio de Ciencia y Tecnología under contract PNE−002/2000−C.

References

A'Hearn, M. F., Schleicher, D. G., Millis, R. L., et al. 1984, AJ, 89, 579

A'Hearn, M. F., Hoban, S., Birch, P. V., et al. 1986, Nature, 324, 649
A'Hearn, M. F., Millis, R. L., Schleicher, D. G., et al. 1995, Icarus, 118, 223
Altenhoff, W. J., Batrla, W. K., Huchtmeier, W. K., et al. 1983, A&A, 125, L19
Arpigny, C. 1994, in AIP Conf. Proc., 312, 205
Biver, N., Bockelée-Morvan, D., Crovisier, J., et al. 1999, AJ, 118, 1850
Biver, N., Bockelée-Morvan, D., Crovisier, J., et al. 2002, EMP, 90, 323,
Bockelée-Morvan, D., & Crovisier, J. 1985, A&A, 151, 90
Boehnhardt, H. 2002, Earth, Moon and Planets, 89, 91
Boehnhardt, H., & Birkle, K. 1994, A&AS, 107, 101
Bonev, T., & Jockers, K. 2002, ESA-SP, 500, 587
Churyumov, K. I., Luk'yanyk, I. V., Berezhnoi, A. A., et al. 2002, EMP, 90, 316
Cosmovici, C. B. Schwarz, G. Ip, W.-H., & Mack, P. 1988, Nature, 332, 705
Feldman, P. D., Fournier, K. B., Grinin, V. P., & Zvereva, A. M. 1993, ApJ, 404, 348
Festou, M. C. 1981, A&A, 95, 69
Festou, M. C., Tozzi, G. P., Smaldone, L. A., et al. 1990, A&A, 227, 609
Fink, U., Combi, M. R., & DiSanti, M. A. 1991, ApJ, 383, 356
Hamuy, M., Walker, A. R., Suntzeff, N. B., et al. 1992, PASP, 104, 533
Hanner, M. S. 1981, Icarus, 47, 342
Haser, L. 1957, Bull. Cl. Sci. Acad. R. Belg., 43, 740
Huebner, W. 1981, in Comets and the origin of life (Dordrecht, D. Reidel Publishing Co.), 91
Huebner, W. F., Keady, J. J., & Lyon, S. P. 1992, Ap&SS, 195, 1
Huebner, W. F., & Link, R. 1999, http://espsun.space.swri.edu/spacephysics/atomic/html/photoabs.htm
Kolokolova, L., Lara, L. M., Schulz, R., Stüwe, J. A., & Tozzi, G. P. 2001, Icarus, 153, 197
Krasnopolsky, V. A. 1991, A&A, 245, 310
Lara, L. M., Schulz, R., Stüwe, J. A., & Tozzi, G. P. 2001, Icarus, 150, 124
Lara, L. M., Licandro, J., di Martino, M., & Tozzi, G. P. 2002, ESA-SP, 500, 709
Larson, S., Sekanina, Z., Levy, D., et al. 1987, A&A, 187, 639
Palmer, P., Wootten, A., Butler, B., et al. 1996, A&AS, 188, 621
Richter, G. M. 1978, Astron. Nachr. 299, 283
Richter, G. M. 1991, Proc. 3rd ESO Workshop on Data Analysis, 37
Roettger, E. E. 1991, Ph.D. Thesis, John Hopkins University, Baltimore, Maryland
Schleicher, D. G. 1983, Ph.D. Dissertation, Univ. of Maryland
Schleicher, D. J., Millis, R. L., & Birch, P. V. 1987, A&A, 187, 531
Schleicher, D. G., Woodney, L. M., & Birch, P. V. 2002, EMP, 90, 401
Schulz, R. 1991, Proc. 3rd ESO/ST-ECP Data Analysis Workshop, 73
Schulz, R., A'Hearn, M. F., Birch, P. V., et al. 1993, Icarus, 104, 206
Schulz, R., Stüwe, J. A., Tozzi, G. P., & Owens, A. 2000, A&A, 361, 359
Szabó, G. M., Kiss, L. L., Sárneczky, & Sziládi, K. 2002, A&A, 384, 702
Tegler, A., & Wyckoff, H. 1989, ApJ, 343, 445
Tozzi, G. P., & Festou, M. C. 1990, in Asteroids, Comets and Meteors III (Langerkvist, Rickman, Lindblad and Lindgren Eds), Upsala Universitet, 463
Tozzi, G. P., & Licandro, J. 2002, Icarus, 157, 187
Tozzi, G. P., Boehnhard, H., Campins, H., et al. 2002, ESA-SP 500, 593
Tozzi, G. P., Lara, L. M., Kolokolova, L., et al. 2004, A&A, in press
Turner, N. J., & Smith, G. H. 1999, AJ, 118, 3039
Watanabe, J. 2001, IAU Circ., 7762